Effect of Laser Remelting on Microstructure and Properties of AlCoCrFeNi High-Entropy Alloy Coating

Qi Liu, Tian-shun Dong, Bin-guo Fu, Guo-lu Li, and Li-jun Yang

A high-entropy alloy coating of AlCoCrFeNi was prepared by plasma spraying and then remelted via laser remelting. The effect of laser remelting on the microstructure, mechanical properties and wear resistance of the AlCoCrFeNi coating was investigated. Particularly, the effect of surface free energy on the wear resistance of the coatings before and after remelting was explored. The results showed that the remelted AlCoCrFeNi coating retained the same single BCC solid solution structure as the as-sprayed AlCoCrFeNi coating. Besides, the defects in the coating were basically eliminated by laser remelting, leading to the porosity of the coating decreased from 4.8 to only 0.3%. Consequently, the hardness, elastic modulus and fracture toughness of the coating were enhanced by 38%, and the wear loss of the remelted AlCoCrFeNi coating was only 22% of that of the as-sprayed one. Therefore, laser remelting is a feasible method to improve the microstructure and enhance the wear resistance of the AlCoCrFeNi high-entropy alloy coating.

1. Introduction

As a new type of alloy, high-entropy alloy has attracted more and more attention of scholars by virtue of its stable structure, high hardness, high wear resistance, excellent corrosion resistance and good thermal stability, which are superior to other traditional alloys (Ref 1-4). However, since the high-entropy alloy generally contains such elements as nickel, cobalt and chromium, and it needs many times of melting to achieve chemical uniformity (Ref 5, 6), the cost of block high-entropy alloy is too high. So the application of high-entropy alloy is greatly limited (Ref 7-9).

Preparing high-entropy alloy coating is considered to be a promising method to promote the industrialization of high-entropy alloy. At the moment, the main preparation methods of high-entropy alloy coating are plasma spraying (Ref 10), laser cladding (Ref 11), mechanical alloying (Ref 12) and electric spark deposition (Ref 13). Among them, plasma spraying is a widely used method to prepare high-entropy alloy coating due to its high temperature, good melting of various refractory materials, wide range of spraying materials and large spraying area (Ref 14, 15). However, the inherent microdefects, e.g., pores and cracks in the plasma sprayed coating, and the weak bonding between the coating and the substrate dramatically limit the improvement in

high-entropy alloy coating performance (Ref 16). Therefore, it is necessary to remelt the high-entropy alloy coating. Wang (Ref 17) explored the solidification cracking mechanism of CrMnFeCoNi high-entropy alloy coating under different laser remelting parameters and different solidification mode types; Cai (Ref 18) prepared NiCrCoTiV high-entropy alloy coating combining with laser cladding and laser remelting. The results show that the phase composition of the coating remains unchanged, and the microstructure and properties of the coating are improved after remelting. However, there are few reports about laser remelting after plasma spraying high-entropy alloy coating up to now.

In addition, as an important characteristic of material surface, surface free energy has an important influence on many physical and chemical properties of materials. For the coatings under the condition of friction and wear, because the change of surface free energy and its component can affect the adhesion characteristic between the coating and the counter grinding pair, it will directly affect the wear resistance of the coatings. However, few investigation has been conducted according to the change of surface free energy of coatings before and after remelting. So the relationship between the surface free energy and the wear resistance of coatings before and after remelting is not clear (Ref 19).

In this study, a high-entropy alloy coating of AlCoCrFeNi was prepared by plasma spraying and then remelted via laser remelting process, whereupon the microstructure, mechanical properties and wear resistance of the coatings before and after remelting were studied comparatively, and the effect of surface free energy on the wear resistance of the coatings before and after remelting was explored, which has reference value for the popularization and application of high-entropy alloy coating with high wear resistance.

Qi Liu, Bin-guo Fu, and **Guo-lu Li**, School of Materials Science and Engineering, Hebei University of Technology, Tianjin 300130, China; **Tian-shun Dong**, School of Materials Science and Engineering, Hebei University of Technology, Tianjin 300130, China; and Hebei wear resistant metal casting technology innovation center, Chengde 067000, Hebei, China; **Li-jun Yang**, School of Materials Science and Engineering, Tianjin University, Tianjin 300130, China. Contact e-mails: dongtianshun111@163.com and liguolu0305@163.com.

2. Experimental Methods

2.1 Coatings Preparation

The raw materials were Al, Co, Cr, Fe and Ni spherical powder with equal molar ratio, whose size was 45-105 μm and

was prepared by gas atomization. AISI 1045 steel was selected as the substrate with chemical composition (wt.%) of 0.42-0.50 C, 0.17-0.37 Si, 0.50-0.80 Mn, ≤ 0.25 Cr, ≤ 0.30 Ni and ≤ 0.25 Cu. Before plasma spraying, the substrate was cleaned with acetone to remove oil stain and sandblasted on the surface. GP-80 plasma spraying equipment and BF-02 powder feeder were used to prepare the coating. The coating thickness was 300 μm. The plasma spraying parameters were as follows: Voltage was 70V, current was 500A, spraying distance was 100 mm, gas flow rate was 80L/min, and powder feeding rate was 40g/min. Then, laser remelting was carried out on the as-sprayed coating, and the equipment model was YLS-10000-S4. Laser remelting parameters were as follows: Power was 1200W, scanning speed was 10mm/s, spot size was 5mm, and argon flow rate was 20L/min.

2.2 Sample Characterization

The microstructure and element analysis of the AlCoCrFeNi coatings before and after remelting were carried out by a scanning electron microscope of lanthanum hexaborate (SEM, Japan Electronic JSM-6510A) and an energy-dispersive spectrometer (EDS). The porosities of the AlCoCrFeNi coatings before and after remelting were measured by Imagej2x software. XRD was used to analyze the phase of the coatings before and after remelting. The scanning range was 10°~90°, and the scanning speed was 6°/min. The microhardness of the AlCoCrFeNi coatings before and after remelting was measured by a Shimadzu HMV-2t Vickers microhardness tester. The load was 1.96N and the residence time was 10s. The elastic modulus was measured by XP + DCM nanoindentation instrument. The contact angles of the AlCoCrFeNi coatings before and after remelting were measured by OCA-30 automatic contact angle measuring instrument. Distilled water, ethylene glycol and diiodomethane were selected as probe liquids. The surface free energy of the AlCoCrFeNi coatings before and after remelting was calculated by Berthelot (Ref 20, 21).

2.3 Wear Tests

The wear resistance of the AlCoCrFeNi coatings before and after remelting was tested by UMT-3 multifunctional friction and wear tester. GCr15 ball with a diameter of 4 mm was used as the counter grinding pair, whose Rockwell hardness was 61 HRC. In order to ensure the consistency of the experimental conditions, the samples were ground with SiC abrasive paper from #400 to #2000. The experimental parameters were as follows: The load was 10N, frequency was 4 Hz, duration time was 20 min, and amplitude was 5 mm. The three-dimensional morphology and wear volume loss of the AlCoCrFeNi coatings before and after remelting were measured by phase-shifting MicroXAM-3D topography instrument.

3. Results and Discussion

3.1 Cross-Sectional Morphology and Microstructure of the COATINGS

Figure 1 shows the cross-sectional morphology of AlCoCrFeNi high-entropy alloy coatings before and after remelting, as well as the microstructure of the AlCoCrFeNi coating after remelting. It can be clearly seen from Fig. 1(a) that the as-

sprayed AlCoCrFeNi coating was layered structure, in which there were many pores and cracks. And there were some unmelted particles and uneven cracks at the interface; the coating and the substrate were typical mechanical combination. It can be seen from Fig. 1(b) that defects in the AlCoCrFeNi coating were basically eliminated after remelting, and the coating structure became uniform and dense. The AlCoCrFeNi coating after remelting was closely bonded with the substrate, and the interface was metallurgical bonding. Analyzed by the ImageJ2x software, the porosity of the as-sprayed AlCoCrFeNi coating was 4.8%, and that of the remelted AlCoCrFeNi coating was only 0.3%. Therefore, the compactness of AlCoCrFeNi coating was greatly improved by remelting.

The microstructure of remelted AlCoCrFeNi coating is shown in Fig. 1(c) and (d). It can be seen that the microstructure was a simple structure composed of dendrites, and no obvious intermetallic compounds or other products were found. The EDS composition analysis of the microstructure in Fig. 1(d) is shown in Table 1. It can be seen that the content of Al element in dendrite was obviously higher than that in interdendrite region, while the segregation of Fe occurred in the interdendrite region. The element content in AlCoCrFeNi coating before and after remelting is shown in Table 1, indicating that only a small amount of Fe element in the substrate entered the coating during laser remelting, and its composition content still conformed to the composition design of high-entropy alloy coating.

3.2 Entropy Value Calculation

In order to further determinate whether the remelted AlCoCrFeNi coating belongs to high-entropy coating, its entropy value was calculated. In statistical thermodynamics, entropy is a parameter representing the disorder degree of the system. The more chaotic the system is, the higher the entropy is; at the same time, it is easier to form solid solution. According to Boltzmann hypothesis, the mixing entropy of alloy system can be expressed as follows (Ref 22):

$$\Delta S_{\text{conf}} = -R \sum_1^n x_i \ln x_i \qquad \text{(Eq 1)}$$

where R=8.314 j/(k·mol), x_i is the content of the ith element (at.%) and n is the number of elements. The content of elements in the coating before and after remelting was analyzed by EDS, as shown in Table 1. It can be seen that the element content of the as-sprayed coating was close to the set equiatomic ratio, and its mixing entropy value was 1.6089R. After remelting, the iron content in the coating increased slightly, and the entropy value of the remelted coating was 1.5989R, indicating that the entropy value decreased, but the variation was not much, which still conformed to the definition of high-entropy alloy. According to Gibbs free energy formula (Ref 22):

$$\Delta G_{\text{mix}} = \Delta H_{\text{mix}} - T\Delta S_{\text{mix}} \qquad \text{(Eq 2)}$$

It was obvious that high mixing entropy can effectively reduce the free energy of the total system and improve the stability of the high-entropy alloy coating. During the solidification process of the high-entropy alloy coating, the alloying atoms were randomly distributed on the lattice positions of the lattice, reducing the degree of the atoms ordering and segregation, inhibiting the formation of ordering intermetallic
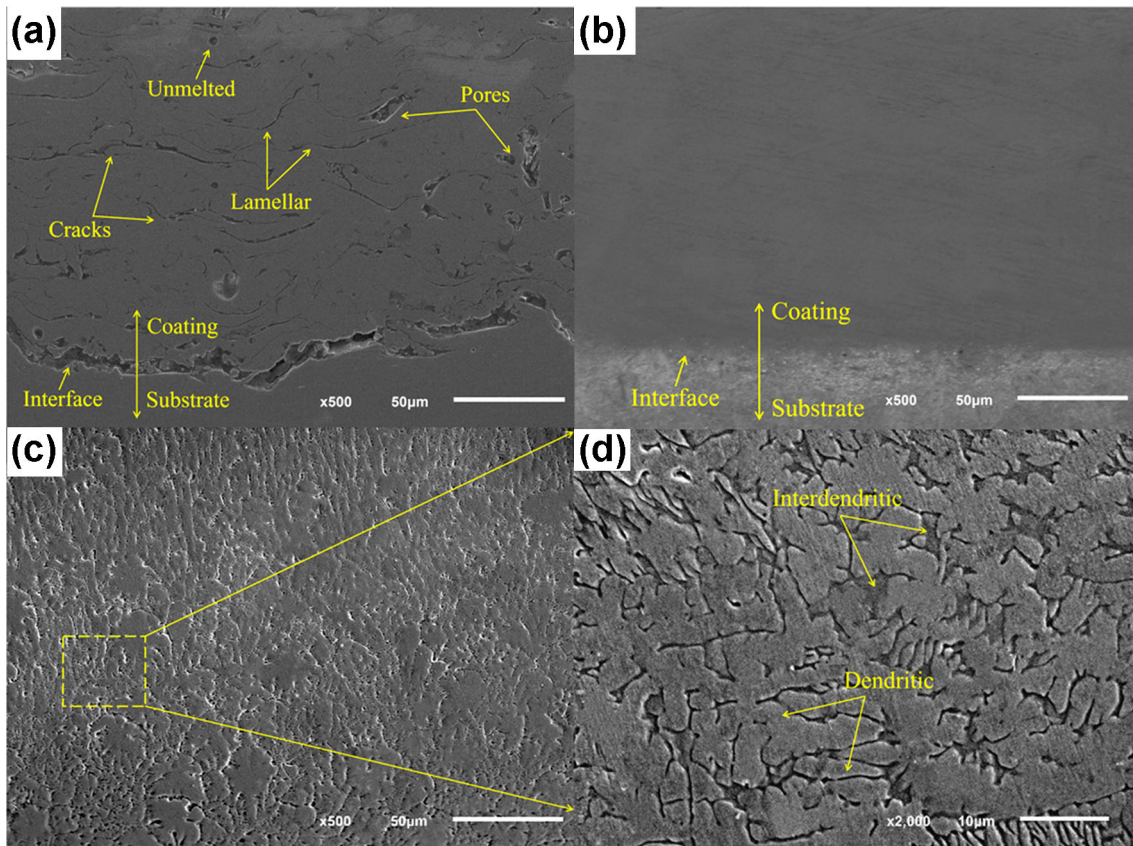
Fig. 1 SEM image of coating: (a) as-sprayed coating, (b) remelted coating, (c), (d) microstructure of remelted coating

Table 1 EDS composition analysis

Region	Al	Co	Cr	Fe	Ni
As-sprayed coating	20.49	18.93	20.56	21.08	19.04
Remelted coating	15.98	18.82	20.32	26.31	18.57
Dendrite	16.84	20.09	20.45	22.92	19.72
Interdendrite	12.08	20.38	21.16	26.30	20.09

compounds, and leading to the multi-principal component solid solution was easier to produce and more stable (Ref 23, 24).

3.3 XRD Analysis of the Coatings

The XRD patterns of the AlCoCrFeNi high-entropy alloy coatings before and after remelting are shown in Fig. 2. The as-sprayed coating presented a single BCC structure, which was mainly attributed to the high-entropy effect of the high-entropy alloy coating. It can increase the compatibility between the main components and reduce the tendency of ordering and segregation (Ref 25-27). Therefore, almost no intermetallic compounds were found in the AlCoCrFeNi coatings before and after remelting. Compared with the as-sprayed AlCoCrFeNi coating, the phase composition of the remelted AlCoCrFeNi coating has no significant change, and the main peak strength was significantly enhanced, which was due to the recrystallization of the coating after complete melting during the remelting process. At the same time, the Al element which was easy to be combined with oxygen was oxidized during
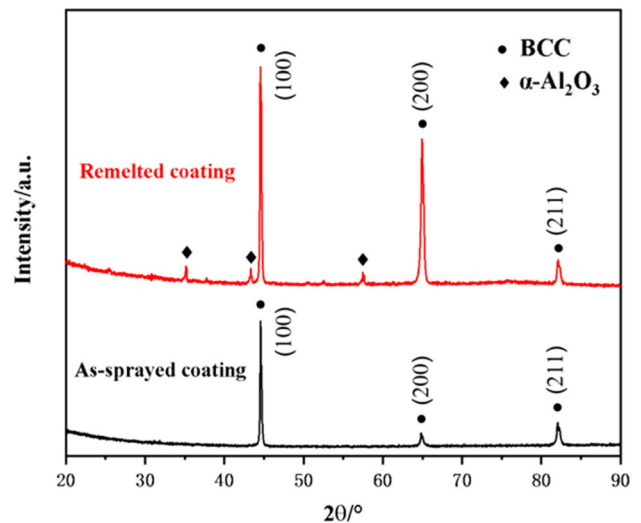

Fig. 2 XRD patterns of coatings before and after remelting

remelting, leading to a small amount of α-Al_2O_3 was detected in the remelted AlCoCrFeNi coating.

3.4 Mechanical Properties

Figure 3 shows the cross-sectional microhardness curves of AlCoCrFeNi coating before and after remelting. It was evident that the hardness of both coatings was obviously higher than that of AISI 1045 steel ($245HV_{0.2}$). The average hardness of as-sprayed AlCoCrFeNi coating was $420HV_{0.2}$, while that of

remelted AlCoCrFeNi coating was 580HV$_{0.2}$, or an increase in hardness of 38%. Moreover, the fluctuation of the latter was smaller than that of the former, which can be attributed to the pores and cracks in the as-sprayed coating. Then, the pores and cracks were nearly eliminated via laser remelting, and the microstructure of AlCoCrFeNi coating became more uniform and dense (as indicated in Fig.1). Besides, it was worth noting that there was a transition zone of about 600 μm between the remelted AlCoCrFeNi coating and the substrate, where the elements dissolved and diffused, which is the characteristic of metallurgical bonding (Ref 28).

The elastic modulus is a measure of the stress required to stretch the internal structure of a metal. The stronger the bonding force between atoms, the greater the elastic modulus. Unlike hardness measurement, the elastic modulus was measured by nanoindentation during unloading, so it was more sensitive even at lower penetration depth (Ref 29). Figure 4 shows the load displacement curves of the two coatings. The average elastic modulus of the as-sprayed AlCoCrFeNi coating was 129 GPa, while that of the remelted AlCoCrFeNi coating

was 197GPa. Furthermore, the measurement results of the as-sprayed coating were biased, while the three measurements of the remelted coating were similar. These can be attributed to the structure of the remelted coating was more uniform and dense.

The fracture toughness of coatings is an important index to measure the properties of coatings. The calculation formula is as follows (Ref 30, 31):

$$K_{IC} = \delta \times \left(\frac{E}{HV} \right)^{1/2} \times \frac{P}{C^{3/2}} \left(MPa \cdot m^{1/2} \right) \qquad \text{(Eq 3)}$$

where p is the pressure test load (kgf), C is the indentation crack length (mm), E is the elastic modulus (GPa), H is the microhardness (HV$_{0.1}$), and $\delta = 0.016$. Since the toughness of the AlCoCrFeNi coating after remelting was improved, a larger load was used to collect the crack length. Figure 5 shows the indentation morphology of as-sprayed AlCoCrFeNi coating under 500g load and that of the remelted AlCoCrFeNi coating under 2000g load. It can be seen that there were more cracks on the edge of the indentation of the as-sprayed AlCoCrFeNi coating, while the indentation of the remelted AlCoCrFeNi coating was regular and the cracks were still short even under a larger load, indicating that the toughness of the coating has been greatly improved. According to the calculation, the fracture toughness of as-sprayed AlCoCrFeNi coating was 5.93 MP·m$^{1/2}$, and that of remelted AlCoCrFeNi coating was 186.47 MPa·m$^{1/2}$, or an increase by 30 times. The higher fracture toughness means stronger ability to resist cracks propagation and lower spalling tendency of debris in the process of wear, which is conducive to the improvement in wear resistance of coating.

3.5 Surface Free Energy

For any material, the exchange of material and energy is realized through the coating surface; therefore, it is of great significance to study the physical properties and energy state of the coating surface. The contact angle method is considered to be the most direct and effective method to measure the surface energy of solids[30]. This method is essentially based on the Young's equation describing the solid–liquid–gas interface system, the surface free energy of AlCoCrFeNi coatings before
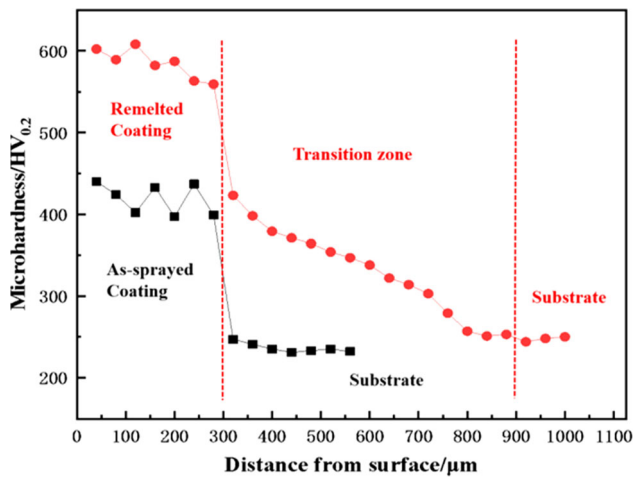

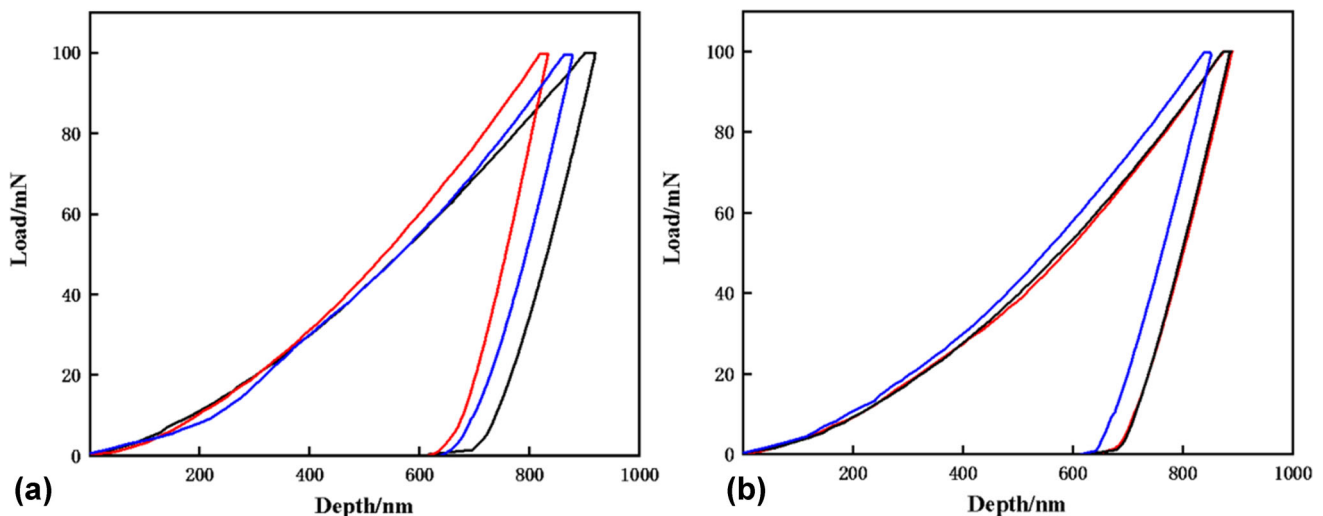**Fig. 3** Cross-sectional microhardness curves of coating before and after remelting

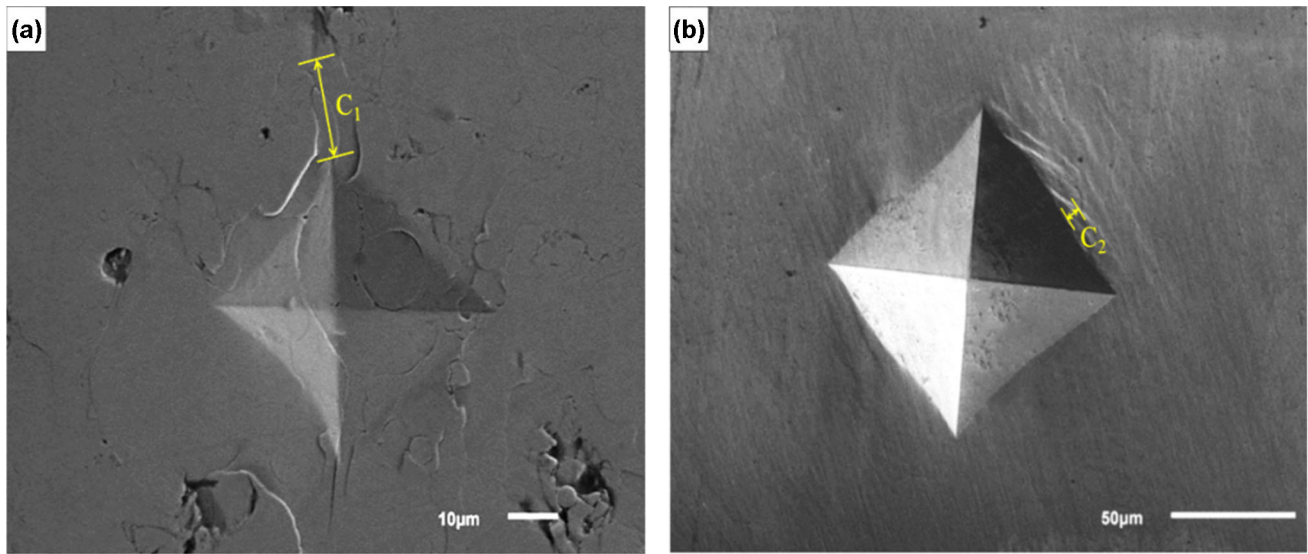**Fig. 4** Load–displacement curves: (a) as-sprayed coating; (b) remelted coating

Fig. 5 Crack morphology: (a) as-sprayed coating, (b) remelted coating

Table 2 Contact angle and surface free energy

	Contact angle, °			Surface free energy, mJ·m^{-2}
Sample	Distilled water	Glycol	Diiodomethane	γ_S
As-sprayed coating	84.70	70.04	56.96	24.54
Remelted coating	102.87	82.35	64.70	18.79

and after remelting was calculated by Berthelot rule, and the calculation formula is as follows (Ref 32):

$$\cos\theta = 2\sqrt{\frac{\gamma_{sv}}{\gamma_{lv}}}[1 - \beta(\gamma_{lv} - \gamma_{sv})^2] \qquad \beta = 1.057 \times 10^{-4} m^2/mJ$$

(Eq 4)

where θ is the contact angle measured by different probes liquids, γ_{lv} is the known surface energy of the liquid, γ_{sv} is the measured surface free energy of solid and liquid, and $\beta = 1.057 \times 10^{-4} m^2/mJ$ is a constant. According to the contact angle data of the AlCoCrFeNi coatings before and after remelting in Table 2, it can be concluded that the surface free energy of the remelted AlCoCrFeNi coating was smaller than that of the as-sprayed AlCoCrFeNi coating. The higher the surface free energy of the coating, the more active the atoms in the surface layer, which makes the coating and the counter grinding pair bond in a small area, thus increasing the friction coefficient of the coating and aggravating its peeling failure.

3.6 Wear Performance

Figure 6(a) shows the friction coefficient curves of the AlCoCrFeNi coatings before and after remelting. It can be seen that the as-sprayed AlCoCrFeNi coating entered stable wear stage at about 200s. Its friction coefficient fluctuated greatly and was maintained at about 0.7, with a gradual upward trend. This was due to brittle fracture and peeling off occurred during wear process, leading to the surface of the as-sprayed coating became uneven. The remelted AlCoCrFeNi coating entered the stable wear stage at about 50s, and its friction coefficient was relatively stable and was maintained at about 0.45. This can be attributed to the high hardness and fracture toughness of the remelted AlCoCrFeNi coating led to less spalling in the wear process.

Figure 6(b) shows the average value of weight loss results of three times of wear. The wear weight loss of the as-sprayed AlCoCrFeNi coating was 2.7mg, whereas that of the remelted AlCoCrFeNi coating was only 0.6mg. The wear loss of remelted AlCoCrFeNi coating is only 22% of that of as-sprayed AlCoCrFeNi coating, indicating that the wear resistance of the AlCoCrFeNi coating was obviously improved by remelting treatment.

The 3D morphology of the wear scar of the as-sprayed AlCoCrFeNi coating and remelted AlCoCrFeNi coating is shown in Fig. 7. The wear data show that the wear scar depth of the as-sprayed AlCoCrFeNi coating was 29.9 μm, the width was 0.84 mm, and the wear volume was 4.745×10^7 μm^3. The wear scar depth of the remelted AlCoCrFeNi coating was only 1.81 μm, the width was 0.43 mm, and the wear volume was 2.309×10^6 μm^3. The results of the three measurements are almost the same, which are consistent with this law. It is evident that the wear degree of the latter was obviously less than that of the former.

The SEM image of the wear morphology of the as-sprayed AlCoCrFeNi coating is shown in Fig. 8(a) and (b). It can be seen that serious spalling phenomenon occurred on the surface of the as-sprayed coating, leaving behind many spalling pits and cracks, showing typical fatigue wear characteristic and a small amount of abrasive wear characteristic. Figure 1 shows the cross-sectional morphology of the as-sprayed AlCoCrFeNi
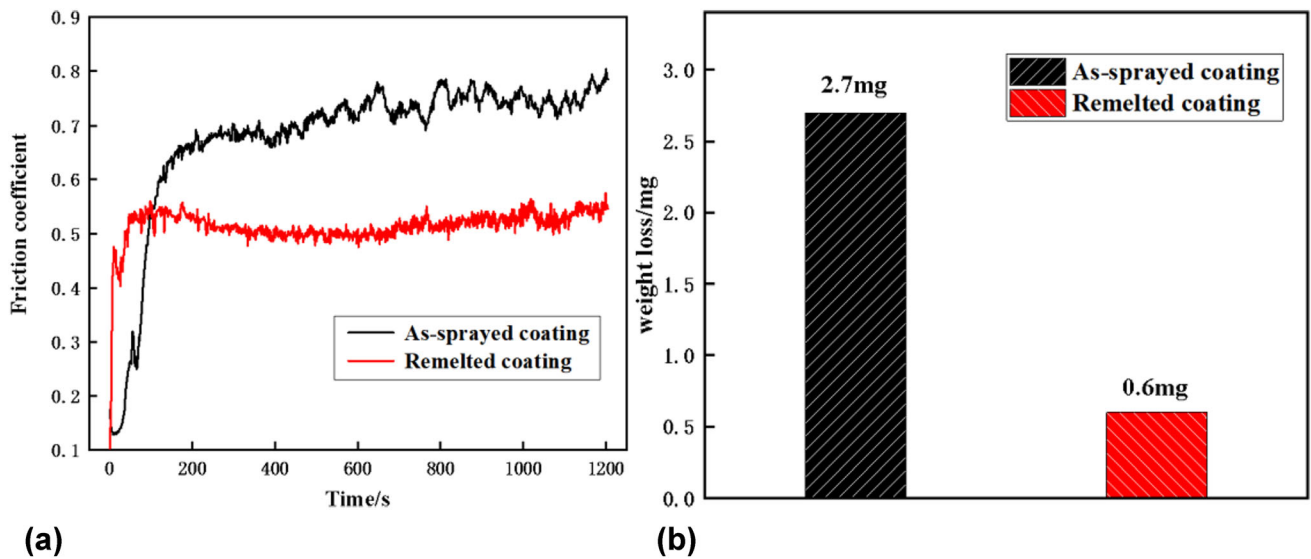
Fig. 6 Friction coefficient and wear loss: (a) friction coefficient curves, (b) the histogram of wear loss
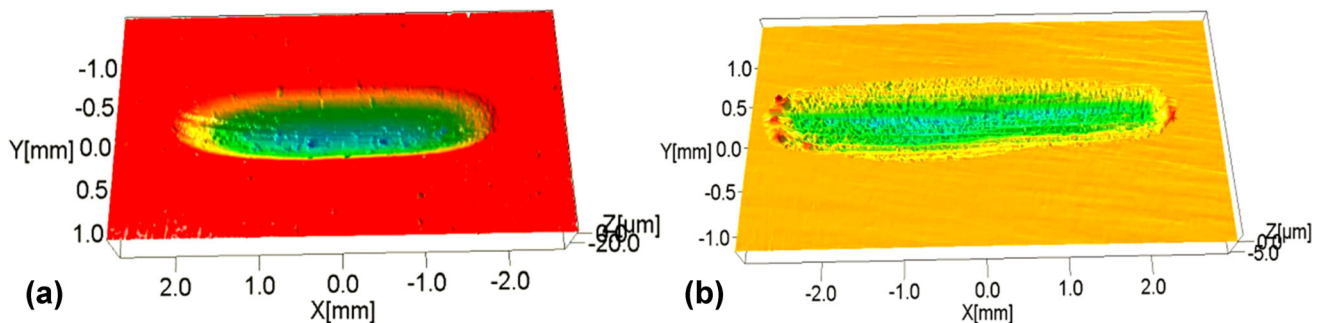

Fig. 7 3D morphology of wear scars: (a) as-sprayed coating, (b) remelted coating

coating. There were many pores and cracks in the as-sprayed AlCoCrFeNi coating which were often the places of stress concentration; thus, it was likely to cause cracks initiation and propagation under the continuous load. When the cracks reached a certain critical length, brittle fracture and spalling would occur under the action of shear force. And we can see a few pieces that were about to peel off, as indicated by the red circle. In addition, by observing the morphology of the spalling pits in Fig. 8(b), it can be found that there were deeper cracks on the right edge of the spalling pits, and the depth of the spalling pits gradually deepened from right to left. According to this, it can be determined that the spalling cracks of fatigue wear were originated from these original cracks on the surface of the as-sprayed AlCoCrFeNi coating. And because the compressive stress was the largest at the subsurface layer of the coating [33], under the action of the pressure stress and shear stress of the grinding pair, the surface cracks extended to the subsurface layer and propagate along the direction parallel to the surface, and finally formed flaky spalling pits.

The wear morphology of the remelted AlCoCrFeNi coating is shown in Fig. 8(c) and (d). It can be seen that the worn surface was full of furrows with a large number of tiny debris on them, which was quite different from the spalling characteristics of the as-sprayed AlCoCrFeNi coating in Fig. 8 (a) and (b). The main reason for the formation of furrows was that the toughness of the AlCoCrFeNi coating dramatically increased

after remelting, and the pores and cracks were basically eliminated after remelting; therefore, only a small amount of fine debris was produced, but no large spalling pits were formed in the process of wear.

From the above research results, the wear resistance of the AlCoCrFeNi coating was improved by laser remelting, and the reasons can be explained as follows:

(1) There were a lot of defects in the as-sprayed AlCoCrFe-Ni coating, such as pores and cracks, which were likely to promote the cracks initiation and propagation and thus seriously weaken the wear resistance of the coating. After remelting treatment, these defects in the AlCoCr-FeNi coating were basically eliminated, and the structure became more uniform and dense. This not only led to the hardness, elastic modulus and fracture toughness of the AlCoCrFeNi coating were improved, but also was conducive to the improvement in its wear resistance.

(2) Moreover, the remelted AlCoCrFeNi coating retained the same single BCC solid solution structure as that of the as-sprayed AlCoCrFeNi coating, which was more wear resistant than FCC structure. In addition, a small amount of α-Al$_2$O$_3$ was produced in the remelted Al-CoCrFeNi coating. The α-Al$_2$O$_3$ belongs to the trigonal system and is the most stable phase in the aluminum oxide, with high melting point, high hardness and good
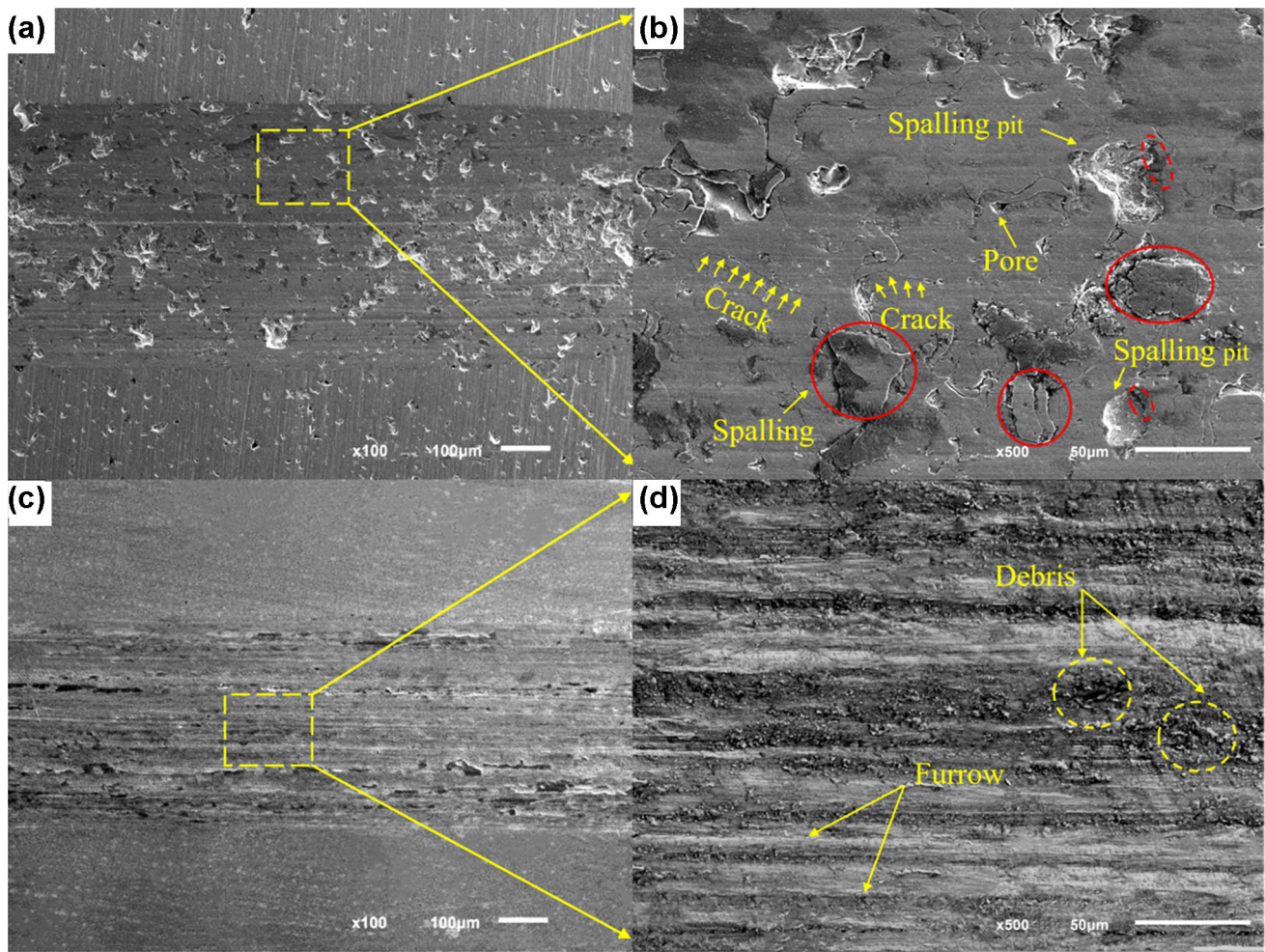
Fig. 8 Wear scar morphology: (a), (b) as-sprayed coating, (c), (d) remelted coating

wear resistance, which made the remelted AlCoCrFeNi coating more wear resistant.

(3) From the point of view of surface free energy, the as-sprayed AlCoCrFeNi coating has higher surface free energy than that of the remelted one, as shown in Table 2. Thus, the convex of the counter grinding pair and coating was likely to form adhesion during the friction process, resulting in a larger friction coefficient and more severe wear of the as-sprayed AlCoCrFeNi coating, as shown in Fig. 6. However, the remelted AlCoCrFeNi coating has lower surface free energy, which can effectively reduce the adhesion between the coating and the counter grinding pair, thus leading to the remelted AlCoCrFeNi coating more wear resistant.

4. Conclusions

The effect of laser remelting on the microstructure, mechanical properties and wear resistance of as-sprayed AlCoCrFeNi high-entropy alloy coating was investigated, and the following conclusions are obtained:

(1) The phases of the AlCoCrFeNi coating changed little after remelting, which was mainly single BCC solid solution structure. The microstructure of the AlCoCrFeNi coating was improved after remelting, the cracks and pores were basically eliminated, thus the porosity of the coating decreased from 4.8 to only 0.3%, and moreover, the mechanical bonding between the coating and the substrate changed into metallurgical bonding.

(2) After remelting, the hardness of the AlCoCrFeNi coating changed from 420 to $580HV_{0.2}$, increased by 38%. The fracture toughness increased by nearly 30 times, which can dramatically reduce the wear loss resulting from fracture mechanism.

(3) The surface free energy of the remelted AlCoCrFeNi coating was lower than that of the as-sprayed AlCoCrFeNi coating, which was beneficial to reducing the adhesion between the coating and the counter grinding pair in the friction process, as well as the spalling or fracture of the coating.

(4) Compared with the as-sprayed AlCoCrFeNi coating, the friction coefficient of the remelted AlCoCrFeNi coating was lower and more stable, and the wear loss was reduced by 77.8%; the wear mechanism of the former was mainly fatigue wear, while that of the latter was abrasive wear.

Acknowledgment

Conflict of interest

The authors declare that they have no known competing financial interests or personal relationships that could have appeared to influence the work reported in this paper.

References

1. S.G. Ma and Y. Zhang, Effect of Nb Addition on the Microstructure and Properties of AlCoCrFeNi High-Entropy Alloy, *Mater. Sci. Eng. A*, 2012, **532**, p 480–486

2. Y. Geng, J. Chen, H. Tan, J. Cheng, and W. Liu, Vacuum Tribological Behaviors of CoCrFeNi High Entropy Alloy at Elevated Temperatures, *Wear*, 2020, **456–457**, p 203368

3. Y. Yu, J. Wang, J. Yang, Z.H. Qiao, H.T. Duan, J.S. Li, J. Li, and W.M. Liu, Corrosive and Tribological Behaviors of AlCoCrFeNi-M High Entropy Alloys Under 90 wt.% H2O2 Solution, *Tribol. Int.*, 2019, **131**, p 24–32

4. J. Dabrowa, G. Cieslak, M. Stygar, K. Mroczka, K. Berent, T. Kulik, and M. Danielewski, Influence of Cu Content on High Temperature Oxidation Behavior of AlCoCrCuxFeNi High Entropy Alloys (x=0; 0.5; 1), *Intermetallics*, 2017, **84**, p 52–61

5. Y.Y. Chen, T. Duval, U.D. Hung, J.W. Yeh, and H.C. Shih, Microstructure and Electrochemical Properties of High Entropy Alloys—A Comparison with type-304 Stainless Steel, *Corros. Sci.*, 2005, **47**(9), p 2257–2279

6. Z.Z. Niu, Y.Z. Wang, C. Geng, J. Xu, and Y. Wang, Microstructural Evolution, Mechanical and Corrosion Behaviors of as-Annealed CoCrFeNiMox (x=0, 0.2, 0.5, 0.8, 1) High Entropy Alloys, *J. Alloy Compd.*, 2020, **820**, p 153273

7. W. Zhang, R. Tang, Z.B. Yang, C.H. Liu, H. Chang, J.J. Yang, J.L. Liao, Y.Y. Yang, and N. Liu, Preparation, Structure, and Properties of an AlCrMoNbZr High-Entropy Alloy Coating for Accident-Tolerant Fuel Cladding, *Surf. Coat. Tech.*, 2018, **347**, p 13–19

8. S. Zhao, L.X. He, X.X. Fan, C.H. Liu, J.P. Long, L. Wang, H. Chang, J. Wang, and W. Zhang, Microstructure and Chloride Corrosion Property of Nanocrystalline AlTiCrNiTa High Entropy Alloy Coating on X80 Pipeline Steel, *Surf. Coat. Tech.*, 2019, **375**, p 215–220

9. P. Shi, Y. Yu, N. Xiong, M. Liu, and Q. Wang, Microstructure and Tribological Behavior of a Novel Atmospheric Plasma Sprayed AlCoCrFeNi High Entropy Alloy Matrix Self-Lubricating Composite Coatings, *Tribol. Int.*, 2020, **151**, p 106470

10. L.H. Tian, W. Xiong, C. Liu, S. Lu, and M. Fu, Microstructure and Wear Behavior of Atmospheric Plasma-Sprayed AlCoCrFeNiTi High-Entropy Alloy Coating, *J. Mater. Eng. Perform.*, 2016, **25**(12), p 5513–5521

11. H.L. Wang, Q.B. Liu, Y.X. Guo, and H.W. Lan, MoFe1.5CrTiWAlNbx Refractory High-Entropy Alloy Coating Fabricated by Laser Cladding, *Intermetallics*, 2019, **115**, p 106613

12. Y. Tian, C.Y. Lu, Y.F. Shen, and X.M. Feng, Microstructure and Corrosion Property of CrMnFeCoNi High Entropy Alloy Coating on Q235 Substrate via Mechanical Alloying Method, *Surf. Interfaces*, 2019, **15**, p 135–140

13. X.R. Wang, Z.Q. Wang, T.S. Lin, and P. He, Mass Transfer Trends of AlCoCrFeNi High-Entropy Alloy Coatings on TC11 Substrate via Electrospark Computer Numerical Control Deposition, *J. Mater. Process. Technol.*, 2017, **241**, p 93–102

14. A. Anupam, R.S. Kottada, S. Kashyap, A. Meghwal, B.S. Murty, C.C. Berndt, and A.S.M. Ang, Understanding the Microstructural Evolution of High Entropy Alloy Coatings Manufactured by Atmospheric Plasma Spray Processing, *Appl. Surf. Sci.*, 2020, **505**, p 144117

15. Y.K. Mu, L.B. Zhang, L. Xu, K. Prashanth, N.Z. Zhang, X.D. Ma, Y.F. Jia, Y.L. Xu, Y.D. Jia, and G. Wang, Frictional Wear and Corrosion Behavior of AlCoCrFeNi High-Entropy Alloy Coatings Synthesized by Atmospheric Plasma Spraying, *Entropy*, 2020, **22**(7), p 740

16. A.S.M. Ang, C.C. Berndt, M.L. Sesso, A. Anupam, S. Praveen, R.S. Kottada, and B.S. Murty, Plasma-Sprayed High Entropy Alloys: Microstructure and Properties of AlCoCrFeNi and MnCoCrFeNi, *Metall. Mater. Trans. A*, 2015, **46**(2), p 791–800

17. C.M. Wang, J.X. Yu, Y. Zhang, and Y. Yu, Phase Evolution and Solidification Cracking Sensibility in Laser Remelting Treatment of the Plasma-Sprayed CrMnFeCoNi High Entropy Alloy Coating, *Mater Design.*, 2019, **182**, p 108040

18. Z.B. Cai, X.F. Cui, Z. Liu, Y. Li, M.L. Dong, and G. Jin, Microstructure and Wear Resistance of Laser Cladded Ni-Cr-Co-Ti-V High-Entropy Alloy Coating After Laser Remelting Processing, *Opt. Laser Technol.*, 2018, **99**, p 276–281

19. N.N. Li, G.L. Li, H.D. Wang, J.J. Kang, T.S. Dong, and H.J. Wang, Influence of TiO2 Content on the Mechanical and Tribological Properties of Cr2O3-Based Coating, *Mater. Design.*, 2015, **88**, p 906–914

20. D.Y. Kwok, and A.W. Neumann, *Contact angle measurement and contact angle interpretation Advances in Colloid and Interface Science.*, 1999, **81**(3), p 167

21. D. Li, and A.W. Neumann, Contact Angles on Hydrophobic Solid Surfaces and Their Interpretation, *J. Colloid Interface Sci.*, 1992, **148**(1), p 190

22. Y. Zhang, T.T. Zuo, Z. Tang, M.C. Gao, K.A. Dahmen, P.K. Liaw, and Z.P. Lu, Microstructures and properties of high-entropy alloys, *Prog. Mater. Sci.*, 2014, **61**, p 15–22

23. Y. Jien-Wei, Alloy Design Strategies and Future Trends in High-Entropy Alloys, *Jom-Us*, 2013, **65**(12), p 1759

24. G. Jin, Z.B. Cai, Y.J. Guan, X.F. Cui, Z. Liu, Y. Li, M.L. Dong, and D. Zhang, High Temperature Wear Performance of Laser-Cladded FeNiCoAlCu High-Entropy Alloy Coating, *Appl. Surf. Sci.*, 2018, **445**, p 113

25. W. Ji, Z.Y. Fu, W.M. Wang, H. Wang, J.Y. Zhang, Y.C. Wang, and F. Zhang, Mechanical Alloying Synthesis and Spark Plasma Sintering Consolidation of CoCrFeNiAl High-Entropy Alloy, *J. Alloy Compd.*, 2014, **589**, p 61–66

26. Y.P. Wang, B.S. Li, M.X. Ren, C. Yang, and H.Z. Fu, Microstructure and Compressive Properties of AlCrFeCoNi High Entropy Alloy, *Mater. Sci. Eng. A*, 2008, **491**(1–2), p 154–158

27. M. Vaidya, A. Prasad, A. Parakh, and B.S. Murty, Influence of Sequence of Elemental Addition on Phase Evolution in Nanocrystalline AlCoCrFeNi: Novel Approach to Alloy Synthesis Using Mechanical Alloying, *Mater. Design.*, 2017, **126**, p 37–46

28. C.Y. Sun, L. Li, M.W. Fu, and Q.J. Zhou, Element Diffusion Model of Bimetallic hot Deformation in Metallurgical Bonding Process, *Mater Design.*, 2016, **94**, p 433

29. S. Mohanty, T.N. Maity, S. Mukhopadhyay, S. Sarkar, N.P. Gurao, S. Bhowmick, and K. Biswas, Powder Metallurgical Processing of Equiatomic AlCoCrFeNi High Entropy Alloy: Microstructure and Mechanical Properties, *Mater. Sci. Eng. A*, 2017, **679**, p 299–313

30. M. Barlet, J.M. Delaye, T. Charpentier, M. Gennisson, D. Bonamy, T. Rouxel, and C.L. Rountree, Hardness and Toughness of Sodium Borosilicate Glasses via Vickers's Indentations, *J. Non-Crystall. Solids*, 2015, **417–418**, p 66

31. R.D. Dukino, and M.V. Swain, Comparative Measurement of Indentation Fracture Toughness with Berkovich and Vickers Indenters, *J. Am. Ceram. Soc.*, 2010, **75**, p 3299–3304

32. Y.M. Liu, J.Y. Shi, Q.Q. Lu, Y.Z. Guo, R.Q. Chen, and D.C. Yin, Research Progress of Solid Surface Energy Calculation Based on Young's Equation, *Mater. Guide*, 2013, **027**(011), p 123–129. (**in Chinese**)

33. Z.Q. Zhang, H.D. Wang, B.S. Xu, and G.S. Zhang, Characterization of Microstructure and Rolling Contact Fatigue Performance of NiCrBSi/WC–Ni Composite Coatings Prepared by Plasma Spraying, *Surf. Coat. Tech.*, 2015, **261**, p 60

Publisher's Note Springer Nature remains neutral with regard to jurisdictional claims in published maps and institutional affiliations.